Editors' Suggestion

Signatures of Enhanced Superconducting Phase Coherence in Optimally Doped $Bi_2Sr_2Y_{0.08}Ca_{0.92}Cu_2O_{8+\delta}$ Driven by Midinfrared Pulse Excitations

F. Giusti,[1,2,*] A. Marciniak,[1,2,*] F. Randi,[1,2] G. Sparapassi,[1,2] F. Boschini,[3,4] H. Eisaki,[5] M. Greven,[6] A. Damascelli,[3,4] A. Avella,[7,8,†] and D. Fausti[1,2,9,‡]

[1]*Department of Physics, Università degli Studi di Trieste, 34127 Trieste, Italy*
[2]*Elettra Sincrotrone Trieste S.C.p.A., 34127 Basovizza Trieste, Italy*
[3]*Department of Physics & Astronomy, University of British Columbia, Vancouver, British Columbia V6T 1Z1, Canada*
[4]*Quantum Matter Institute, University of British Columbia, Vancouver, British Columbia V6T 1Z4, Canada*
[5]*Nanoelectronics Research Institute, National Institute of Advanced Industrial Science and Technology, Tsukuba, Ibaraki 305-8568, Japan*
[6]*School of Physics and Astronomy, University of Minnesota, Minneapolis, Minnesota 55455, USA*
[7]*Dipartimento di Fisica "E.R. Caianiello," Università degli Studi di Salerno, I-84084 Fisciano (SA), Italy*
[8]*CNR-SPIN, UOS di Salerno, I-84084 Fisciano (SA), Italy*
[9]*Department of Chemistry, Princeton University, Princeton, New Jersey 08544, USA*

(Received 6 September 2018; published 15 February 2019)

Optimally doped cuprate are characterized by the presence of superconducting fluctuations in a relatively large temperature region above the critical transition temperature. We reveal here that the effect of thermal disorder, which decreases the condensate phase coherence at equilibrium, can be dynamically contrasted by photoexcitation with ultrashort midinfrared pulses. In particular, our findings reveal that light pulses with photon energy comparable to the amplitude of the superconducting gap and polarized in plane along the copper-copper direction can dynamically enhance the optical response associated with the onset of superconductivity. We propose that this effect can be rationalized by an effective *d*-wave BCS model, which reveals that midinfrared pulses result in a transient increase of the phase coherence.

DOI: 10.1103/PhysRevLett.122.067002

Many of the ingredients required for superconductivity in cuprates survive well beyond the region of the phase diagram where the actual macroscopic superconducting phase resides. An example of this hindered superconductivity is represented by the behavior of underdoped cuprates just above the critical temperature (T_c), where some hints indicate that pairing occurs, but the presence of the superconducting phase is inhibited either by a competing charge order or by the local nature of the pair incoherence (global phase incoherence), blocking the formation of a mesoscopic superconducting state [1–5]. Signatures of an incipient superconductivity at temperatures larger than T_c have been revealed also in optimally doped samples, where the superconducting fluctuations survive tens of Kelvin above the actual T_c [6–17]. The relative fragility of the superconducting phase, together with the underlying presence of its ingredients in large portions of the phase diagram, enables the possibility of controlling superconductivity through ultrashort light pulses.

While there is ample evidence that photoexcitation with ultrashort high photon energy pulses melts the superconducting phase under some specific conditions [6,8,9,18,19], it has been shown that the formation of a superconducting phase can be triggered by midinfrared (MIR) excitations in regions of the phase diagram that are not superconducting at equilibrium [20–24]. The possibility of triggering the onset of quantum coherence through MIR excitations could open up new avenues to control quantum states of matter through light. Here we reveal that the time domain response of optimally doped $Bi_2Sr_2Y_{0.08}Ca_{0.92}Cu_2O_{8+\delta}$ (Y-Bi2212) to excitations with photon energies close to the superconducting gap ($2|\Delta| \approx 75$ meV) is highly anisotropic. While excitations with pump polarization along [100] (the copper-oxygen Cu-O axis) lead to a reduction of the superconducting gap, independent of the photon frequency, photoexcitations along [110] (the copper-copper Cu-Cu axis) seem to trigger an increase of phase coherence, which results in an enhancement of the dynamical response associated with the superconducting phase. The enhancement of the response with [110] excitation is explained within a simple BCS framework, with *d*-wave symmetry for the superconducting gap.

A much debated aspect of superconductivity in cuprates is that the onset of the superconducting phase is followed by a change of spectral weight at an energy scale orders of magnitude larger than the superconducting gap. In particular, in Bi2212, the opening of a superconducting gap at about 35–40 meV is accompained by a spectral weight redistribution at frequencies as high as several eV [25–27].

This is visible in time domain studies where the reflectivity in the visible range changes upon a sudden perturbation of the superconducting gap [28–34]. Here we leverage this characteristic and work under the assumption that the spectral response in the visible-near infrared region is intimately related to the superconductor response.

We performed pump-probe measurements Y-Bi2212. At optimal doping it presents a superconducting phase below $T_c = 97$ K, a pseudogap phase between T_c and $T^* \approx 135$ K and an unusual "strange-metal" phase for higher temperatures [35]. The sample has been excited with MIR ultrashort pulses ($h\nu \approx 70$ meV $\approx 2\Delta$, incident fluence $f = 0.09$ mJ cm^{-2}) obtained through difference frequency generation of two infrared pulses coming from a twin optical parametric amplification system. The transient reflectivity induced by the pump is probed by near-infrared (NIR) pulses ($h\nu \approx$ 1.63 eV) generated by a noncollinear parametric amplifier system. The time delay between the two pulses can be tuned by changing the probe optical path through a μm-translation stage. Both pump and probe propagation directions are parallel to the c axis (that is, perpendicular to the Cu-O layer) and their polarizations were kept parallel in all measurements. External noise contributions to the transient reflectivity are reduced subtracting a reference signal (which does not interact with the sample) to the probe beam. The acquisition has been performed by a lock-in amplifier. More details on the experimental design can be found in the Supplemental Material [36].

The intensity map shown in Fig. 1(a) represents the relative variation of the reflectivity upon the pump excitation as a function of the time delay between the pump and the probe pulses (horizontal axis) and of the temperature of the sample (vertical axis). We focused our investigation in a temperature range from 80 to 110 K. For $T < T_c$, the reflectivity increases for about 1 ps after the arrival of the pump (at 0 ps) and then it starts decreasing through an exponential decay [brown line in Fig. 1(c)]. The characteristic time of the decay increases with temperature, it is maximum at $T = 97$ K (black line) and decreases at higher temperatures. The observed maximum of the time decay is a precise indicator of the superconducting-pseudgap phase transition [19,37].

The anisotropy of the gap of d-wave superconductors suggests a detailed analysis of the effects of excitations with different pump polarizations [38]. Figures 1(a) and 1(b) show the measured transient reflectivity for two different pulse polarizations: along [100] [the Cu-O axis, see Fig. 1(a)] and [110] [the Cu-Cu direction, see Fig. 1(b)]. We measured the transient reflectivity in both polarizations, using a pump photon energy around the characteristic energy of the system in the superconducting phase, that is $2|\Delta| \approx 75$ meV [39]. A convenient way to visualize the polarization dependence of our measurements is to subtract the two maps in Figs. 1(a) and 1(b), as displayed in the differential map of Fig. 2(a). The difference map reveals a sizable signal around T_c, for time

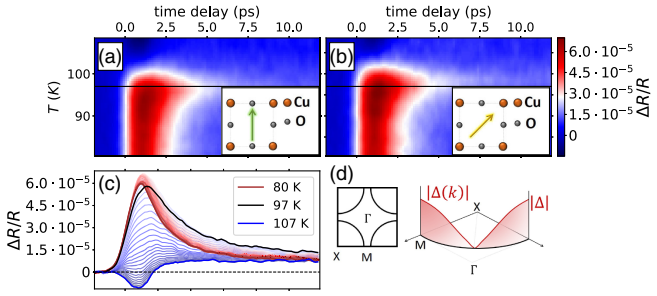

FIG. 1. MIR pump, optical probe measurements. (a) and (b) Reflectivity variation due to an impulsive excitation at time delay 0 ps by a MIR pulse ($h\nu \approx 70$ meV) as a function of the temperature of the sample (vertical axis). The two maps differ in the polarization of the impinging pump, as highlighted by the two insets, representing the direction of the polarization (green and orange arrow) in the Cu-O plane. (c) Time resolved signal at fixed temperatures for Bi2212: the brown line represents the characteristic superconductive signal, while the blue one refers to the pseudogap phase. The transition between the two phases is marked with the black line and is related to the maximum of the time decay. Light colored lines represent intermediate temperatures. (d) Sketch of the first Brillouin zone and of the superconducting d-wave gap amplitude $|\Delta(\mathbf{k})|$ in the reciprocal space. The black curved lines represent the Fermi surface.

delays from 0 to 2 ps, corresponding to the maximum response in the superconducting phase [red region at about 1 ps in Fig. 2(a)].

The result is confirmed by the visual inspection of the temperature dependence at a fixed time delay (1 ps) for different polarizations of the pump, as shown in the inset of Fig. 2(a).

We observe an increase of response associated with the onset of the superconductivity when the pump is polarized

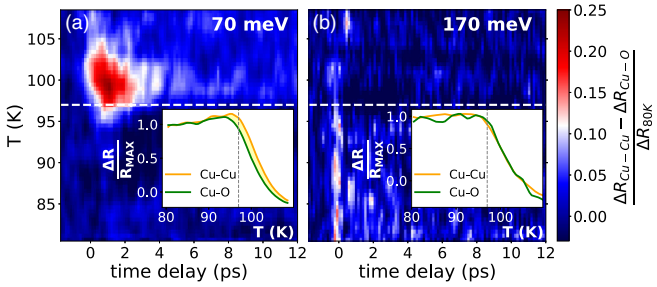

FIG. 2. Wavelength dependent anisotropy. Difference between the transient reflectivities due to Cu-Cu and Cu-O polarized pump in time (horizontal axis) and temperature (vertical axis), induced by excitations with (a) 70 and (b) 170 meV pump photon energies. The dashed lines highlight the critical temperature $T_c = 97$ K. The insets represent the response as a function of temperature at 1 ps time delay for Cu-Cu (orange line) and Cu-O (green line) polarized pump excitations for low and high pump photon energies (a and b, respectively). The gray dashed lines mark T_c. Both in the maps and in the insets the values of the reflectivity have been normalized to the maximum value of the response at 80 K ($\Delta R_{80\,\mathrm{K}}$).

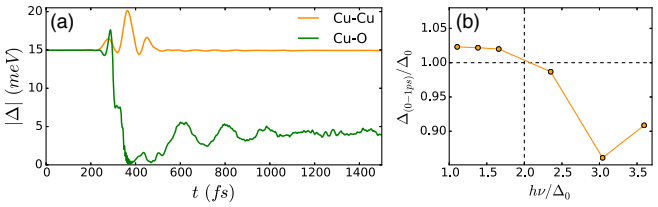

FIG. 3. d-wave BCS microscopic model. Results of the microscopic model: (a) Time evolution of the modulus of the superconducting gap ($|\Delta|$) in both Cu-Cu (orange line) and Cu-O (green line) excitation case. The maximum of the pump electric field is reached at about 350 fs. (b) Normalized integral of $|\Delta|$ in the time interval from 0 to 1 ps as a function of the pump photon energy ($\Delta_0 = |\Delta(t=0)|$) for Cu-Cu polarized pump excitations.

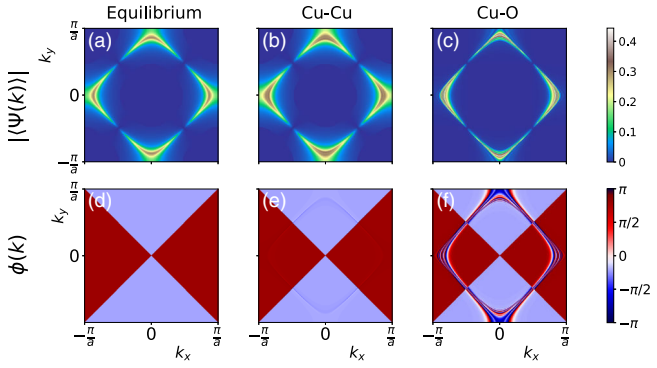

FIG. 4. Time dependent pair operator representation. (a)–(c) Modulus of the expectation value of the pair operator $\hat{\Psi}(\mathbf{k})$ in the reciprocal space in three different situations: (a) No excitation ("Equilibrium"), (b) During a pump excitation polarized along the Cu-Cu and (c) Cu-O direction. Analogously, pictures from (d) to (f) show the phase $\phi(\mathbf{k})$ of $\langle\hat{\Psi}(\mathbf{k})\rangle$, in the same three conditions.

along the Cu-Cu direction both above and below $T_c = 97$ K. We stress that this is an anisotropic response strongly dependent on the photoexcitation wavelength: in Fig. 2(b) we display the differential map retrieved for higher pump photon energy ($h\nu \approx 170$ meV), which reveals no anisotropy at any temperature. This result has been also confirmed by measurements at high pump fluence (see Fig. S4 of the Supplemental Material [36]) demonstrating that the superconducting signal can be increased by a pump polarized along the Cu-Cu axis at long wavelength whereas higher photon energy excitations suppress this effect.

In order to draw a picture of the possible physical scenario emerging from the anisotropic response to low photon energy ultrashort pulses, we implemented a microscopic description based on a generalized BCS Hamiltonian allowing for a k-dependent d-wave gap (for further details see the Supplemental Material [36]). While it is well known that a simple BCS formalism, disregarding first and foremost the presence of electronic correlations, cannot explain the whole cuprate phenomenology, we will argue here that it accounts well for the nonequilibrium response of the low-energy superconducting gap, at least at a qualitative level. From the described Hamiltonian [see Supplemental Material [36], Eq. (1)], it is possible, through density matrix formalism, to calculate the time evolution of several meaningful quantities (such as the superconducting gap amplitude $|\Delta|$).

The model predicts different behaviors depending on the frequency and the polarization of the pump pulse. In particular, Fig. 3(a) shows that low photon energy excitations with polarization parallel to the Cu-Cu direction are predicted to drive an instantaneous enhancement of the superconducting gap, while a pump polarization rotated 45° induces a dynamical quench of the gap. These results qualitatively rationalize the experimentally observed enhancement of the positive signal associated with the superconducting response, triggered by photoexcitation polarized along the Cu-Cu direction for pump photon energy $h\nu \approx 2|\Delta|$. On the other hand, the collapse of the superconducting signal in the Cu-Cu polarization configuration is predicted for higher pump photon energies, as shown in Fig. 3(b), where we display the transient decreases of $|\Delta|$ as a function of the pump photon energy.

In order to grasp the physical picture that emerges from this microscopic model, we calculated the expectation value of the pair operator $\hat{\Psi}(\mathbf{k})$ (see Supplemental Material [36]).

Figure 4 displays the modulus and the phase of the pair amplitude (in the first Brillouin zone) calculated in three different cases: at equilibrium and during a Cu-Cu and Cu-O low photon energy excitation ($h\nu \approx 2\Delta$). We observe that the value of $|\langle\hat{\Psi}(\mathbf{k})\rangle|$ around the Fermi surface is nearly unperturbed (and actually slightly enhanced) in both excitation schemes [Figs. 4(b) and 4(c)], i.e., that pairing is still present in both cases. On the other hand, the phase reveals a strong anisotropic response [Figs. 4(e) and 4(f)]: the model shows that Cu-O polarized excitations drive intense phase fluctuations, which are responsible for the collapse of $|\Delta|$ shown in Fig. 3(a). Cu-Cu polarized low-photon-energy excitations preserve instead phase coherence and enable an enhanced superconducting dynamical response.

We stress that the calculations were performed at a temperature $T < T_c$, where the amplitude of the superconducting gap $|\Delta|$ has a nonzero equilibrium value. This is an intrinsic limitation of the microscopic BCS model, which does not allow superconducting pairing at temperatures higher than the critical value (T_c). The data instead report a well visible enhancement of the superconducting behavior at temperatures up to ≈10 K above the equilibrium critical temperature T_c [inset of Fig. 2(a)].

In order to extend this effective description to higher temperatures, we propose to run calculations from a modified equilibrium state, whose features are justified in the following, maintaining the BCS framework. Different from standard BCS superconductors, cuprates exhibit signatures of strong superconducting fluctuations at temperatures larger

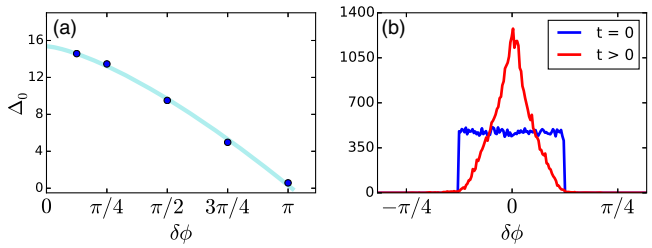

FIG. 5. Extension of the d-wave BCS model above the critical temperature. (a) Values of the superconducting gap at equilibrium [$\Delta_0 = |\Delta|(t = 0)$] as a function of the amplitude of the phase noise. (b) Distribution of the phase values at equilibrium (blue line) and during the excitation polarized along the Cu-Cu direction (red line) for an initial noise amplitude of $\delta\phi = \pi/8$.

than T_c [7]. In particular, in optimally doped Bi2212, both equilibrium and time-domain techniques revealed superconducting fluctuations up to tens of Kelvin above the critical temperature [6,8–10]. This anomalous feature is commonly taken to imply the presence of Cooper pairs losing phase coherence; i.e., while the mesoscopic coherence vanishes above the transition temperature, pairing remains, together with phase correlations, which are local in space and time [7]. Transport [12,13] and magnetization [11] studies suggest that the local correlations lead to a universal superconducting percolative regime above T_c consistent with a percolation picture of the phase diagram [40]; in particular, a local superconducting gap distribution was able to explain [12] the presence of an effective average gap above T_c in photoemission experiments [41] and the exponential tail exhibited by several observables. Here we observe qualitatively the same signatures of local correlations persisting up to ~10 K above T_c, a temperature range similar to previous studies [12,13,40,41].

In order to explore these effects within the generalized BCS model, we employ the following simple procedure. We proposed a new equilibrium state artificially built by adding a random noise to the phase of the original state pair amplitude $\phi(\mathbf{k})$, while retaining its modulus ($|\langle\hat{\Psi}(\mathbf{k})\rangle|$). The phase noise introduced in the model leads to a reduction of the gap, as shown in Fig. 5(a), in which the dependence of the gap amplitude on the maximum value for the phase fluctuations ($\delta\phi$) is plotted. Calculations of the dynamic response, starting from this inhomogeneous (in momentum space) equilibrium state, reveal that Cu-Cu low-photon-energy excitations induce a significant enhancement of phase coherence (and negligible variation in the amplitude) of the pair operator, as highlighted in Fig. 5(b), which depicts a histogram of the phase distribution before (blue line) and during (red line) the photoexcitation (350 fs), for an initial fluctuation of $\delta\phi = \pi/8$ (value chosen for sake of clarity). The plot reveals that the phase distribution, which becomes narrower after the excitation, leads to an enhanced superconducting response. We argue that this scenario rationalizes the enhancement of an out-of-equilibrium superconducting behavior above T_c, which could therefore be associated with a light-driven boost of phase coherence.

The scenario that emerges from our pump-probe experiments reveals the capability to enhance the transient response associated with superconducting fluctuations in cuprates by means of photoexcitations with low-energy photons polarized in the Cu-Cu direction, which is completely suppressed by a pump excitation with polarization parallel to the Cu-O axis. The effective d-wave BCS description of the interaction of the superconductor and pulsed electromagnetic radiation is in qualitative agreement with the experimental results. Moreover it allows us to ascribe the observed dynamical increase of the superconductive response to a light-driven enhancement of phase coherence below and above T_c, where thermodynamic constraints make the superconducting equilibrium state unattainable. On the other hand, it is unclear what will happen in underdoped cuprates, where correlations may play a stronger role. The d-wave BCS model describes well the electrodynamic response of the superconducting phase, but, as discussed, it lacks in describing the effects of strong correlations. Although the discussion of underdoped cuprates is beyond the scope of this work, our conclusions suggest that a field-driven increase of phase coherence may play a role in their response. This opens the intriguing perspective of driving the onset of quantum coherence in these materials by mid-IR excitation.

This research was undertaken thanks in part to funding from the Max Planck-UBC-UTokyo Centre for Quantum Materials and the Canada First Research Excellence Fund, Quantum Materials and Future Technologies Program. The work at UBC was supported by the Killam, Alfred P. Sloan, and Natural Sciences and Engineering Research Council of Canada's (NSERC'S) Steacie Memorial Fellowships (A. D.), the Alexander von Humboldt Fellowship (A. D.), the Canada Research Chairs Program (A. D.), NSERC, Canada Foundation for Innovation (CFI) and CIFAR Quantum Materials Program. The work at the University of Minnesota was funded by the Department of Energy through the University of Minnesota Center for Quantum Materials under DE-SC-0016371. This research was mainly supported by the Italian Ministry of Education (MIUR), through Grant No. RBSI14ZIY2, financed under the Scientific Independence of Young Researchers program (SIR2014).

*These two authors contributed equally.
†Corresponding author.
avella@physics.unisa.it
‡Corresponding author.
daniele.fausti@elettra.eu

[1] T. Timusk and B. Statt, Rep. Prog. Phys. **62**, 61 (1999).

[2] U. Chatterjee, M. Shi, A. Kaminski, A. Kanigel, H. M. Fretwell, K. Terashima, T. Takahashi, S. Rosenkranz, Z. Z. Li, H. Raffy, A. Santander-Syro, K. Kadowaki, M. R. Norman, M. Randeria, and J. C. Campuzano, Phys. Rev. Lett. **96**, 107006 (2006).

[3] R. Daou *et al.*, Nature (London) **463**, 519 (2010).

[4] J. Lee, K. Fujita, A. R. Schmidt, C. K. Kim, H. Eisaki, S. Uchida, and J. C. Davis, Science **325**, 1099 (2009).

[5] S. A. Kivelson, I. P. Bindloss, E. Fradkin, V. Oganesyan, J. M. Tranquada, A. Kapitulnik, and C. Howald, Rev. Mod. Phys. **75**, 1201 (2003).

[6] L. Perfetti, B. Sciolla, G. Biroli, C. J. van der Beek, C. Piovera, M. Wolf, and T. Kampfrath, Phys. Rev. Lett. **114**, 067003 (2015).

[7] J. Corson, R. Mallozzi, J. Orenstein, J. N. Eckstein, and I. Bozovic, Nature (London) **398**, 221 (1999).

[8] I. Madan, T. Kurosawa, Y. Toda, M. Oda, T. Mertelj, P. Kusar, and D. Mihailovic, Sci. Rep. **4**, 5656 (2015).

[9] F. Boschini *et al.*, Nat. Mater. **17**, 416 (2018).

[10] T. Kondo, W. Malaeb, Y. Ishida, T. Sasagawa, H. Sakamoto, T. Takeuchi, T. Tohyama, and S. Shin, Nat. Commun. **6**, 7699 (2015).

[11] G. Yu, D.-D. Xia, D. Pelc, R.-H. He, N.-H. Kaneko, T. Sasagawa, Y. Li, X. Zhao, N. Barišić, A. Shekhter, and M. Greven, arXiv:1710.10957.

[12] D. Pelc, M. Vučković, M. S. Grbić, M. Požek, G. Yu, T. Sasagawa, M. Greven, and N. Barišić, Nat. Commun. **9**, 4327 (2018).

[13] P. Popčević, D. Pelc, Y. Tang, K. Velebit, Z. Anderson, V. Nagarajan, G. Yu, M. Požek, N. Barišić, and M. Greven, Quantum Mater. **3**, 42 (2018).

[14] M. S. Grbić, N. Barisic, A. Dulcic, I. Kupcic, Y. Li, X. Zhao, G. Yu, M. Dressel, M. Greven, and M. Pozek, Phys. Rev. B **80**, 094511 (2009).

[15] L. S. Bilbro, R. V. Aguilar, G. Logvenov, O. Pelleg, I. Božović, and N. P. Armitage, Nat. Phys. **7**, 298 (2011).

[16] J. Orenstein, J. Corson, S. Oh, and J. N. Eckstein, Ann. Phys. (Amsterdam) **15**, 596 (2006).

[17] I. Kokanović, D. J. Hills, M. L. Sutherland, R. Liang, and J. R. Cooper, Phys. Rev. B **88**, 060505(R) (2013).

[18] C. L. Smallwood, W. Zhang, T. L. Miller, C. Jozwiak, H. Eisaki, D. H. Lee, and A. Lanzara, Phys. Rev. B **89**, 115126 (2014).

[19] C. Giannetti, M. Capone, D. Fausti, M. Fabrizio, F. Parmigiani, and D. Mihailovic, Adv. Phys. **65**, 58 (2016).

[20] D. Fausti, R. I. Tobey, N. Dean, S. Kaiser, A. Dienst, M. C. Hoffmann, S. Pyon, T. Takayama, H. Takagi, and A. Cavalleri, Science **331**, 189 (2011).

[21] S. Kaiser, C. R. Hunt, D. Nicoletti, W. Hu, I. Gierz, H. Y. Liu, M. Le Tacon, T. Loew, D. Haug, B. Keimer, and A. Cavalleri, Phys. Rev. B **89**, 184516 (2014).

[22] W. Hu, S. Kaiser, D. Nicoletti, C. R. Hunt, I. Gierz, M. C. Hoffmann, M. Le Tacon, T. Loew, B. Keimer, and A. Cavalleri, Nat. Mater. **13**, 705 (2014).

[23] E. Casandruc, D. Nicoletti, S. Rajasekaran, Y. Laplace, V. Khanna, G. D. Gu, J. P. Hill, and A. Cavalleri, Phys. Rev. B **91**, 174502 (2015).

[24] M. Mitrano *et al.*, Nature (London) **530**, 461 (2016).

[25] H. J. A. Molegraaf, Science **295**, 2239 (2002).

[26] D. N. Basov and T. Timusk, Rev. Mod. Phys. **77**, 721 (2005).

[27] A. V. Boris, N. N. Kovaleva, O. V. Dolgov, T. Holden, C. T. Lin, B. Keimer, and C. Bernhard, Science **304**, 708 (2004).

[28] J. Demsar, B. Podobnik, V. V. Kabanov, Th. Wolf, and D. Mihailovic, Phys. Rev. Lett. **82**, 4918 (1999).

[29] M. Gedik, M. Langner, J. Orenstein, S. Ono, Y. Abe, and Y. Ando, Phys. Rev. Lett. **95**, 117005 (2005).

[30] R. A. Kaindl, M. A. Carnahan, D. S. Chemla, S. Oh, and J. N. Eckstein, Phys. Rev. B **72**, 060510 (2005).

[31] P. Kusar, V. V. Kabanov, J. Demsar, T. Mertelj, S. Sugai, and D. Mihailovic, Phys. Rev. Lett. **101**, 227001 (2008).

[32] C. Giannetti, G. Coslovich, F. Cilento, G. Ferrini, H. Eisaki, N. Kaneko, M. Greven, and F. Parmigiani, Phys. Rev. B **79**, 224502 (2009).

[33] J. Demsar, R. D. Averitt, A. J. Taylor, V. V. Kabanov, W. N. Kang, H. J. Kim, E. M. Choi, and S. I. Lee, Phys. Rev. Lett. **91**, 267002 (2003).

[34] R. D. Averitt, G. Rodriguez, A. I. Lobad, J. L. W. Siders, S. A. Trugman, and A. J. Taylor, Phys. Rev. B **63**, 140502 (R) (2001).

[35] F. Cilento, S. Dal Conte, G. Coslovich, F. Banfi, G. Ferrini, H. Eisaki, M. Greven, A. Damascelli, D. van der Marel, and F. Parmigiani, J. Phys. Conf. Ser. **449**, 012003 (2013).

[36] See Supplemental Material at http://link.aps.org/supplemental/10.1103/PhysRevLett.122.067002 for the description of set-up design, the BCS calculation details and the additional measurements with high excitation fluence.

[37] J. Demsar, R. Hudej, J. Karpinski, V. V. Kabanov, and D. Mihailovic, Phys. Rev. B **63**, 054519 (2001).

[38] T. P. Devereaux and R. Hackl, Rev. Mod. Phys. **79**, 175 (2007).

[39] W. S. Lee, I. M. Vishik, K. Tanaka, D. H. Lu, T. Sasagawa, N. Nagaosa, T. P. Devereaux, Z. Hussain, and Z.-X. Shen, Nature (London) **450**, 81 (2007).

[40] D. Pelc, P. Popčević, M. Požek, N. Barišić, Sci. Adv. **5**, eaau4538 (2019).

[41] T. J. Reber *et al.*, Phys. Rev. B **87**, 060506(R) (2013).

Supplemental Material: Signatures of enhanced superconducting phase coherence through MID-IR excitation in optimally doped Y-Bi2212

F. Giusti,[1,2,*] A. Marciniak,[1,2,*] F. Randi,[1,2] G. Sparapassi,[1,2] F. Boschini,[3,4] H. Eisaki,[5] M. Greven,[6] A. Damascelli,[3,4] A. Avella,[7,†] and D. Fausti[1,2,8,‡]

[1]*Department of Physics, Università degli Studi di Trieste, 34127 Trieste, Italy*
[2]*Elettra Sincrotrone Trieste S.C.p.A., 34127 Basovizza Trieste, Italy*
[3]*Department of Physics and Astronomy, University of British Columbia, Vancouver, Canada*
[4]*Quantum Matter Institute, University of British Columbia, Vancouver, BC V6T 1Z4, Canada*
[5]*Nanoelectronics Research Institute, National Institute of Advanced Industrial Science and Technology, Tsukuba, Ibaraki 305-8568, Japan*
[6]*School of Physics and Astronomy, University of Minnesota, Minneapolis, MN 55455, USA*
[7]*Department of Physics, Università degli Studi di Salerno, 84084 Fisciano (SA), Italy*
[8]*Department of Chemistry, Princeton University, Princeton, New Jersey 08544, United States*

METHODS

Experimental Design

The Laser system is made up of a Non-Collinear Parametric Amplifier (Orpheus-N by Light Conversion) and a Twin Optical Parametric Amplifier (Orpheus TWIN by Light Conversion), both pumped on the Light Conversion Pharos Laser, producing 400 μJ pulses with 1.2 eV photon energy at 50 KHz repetition rate.
The optical probe (generated by the NOPA system) is a $\sim$ 20 fs pulse wavelength tunable in the visible (measurement reported at 760 nm). The carrier envelope phase stable MIR pump pulses are produced by Difference Frequency Generation (DFG) mixing the signal outputs of the twin OPA seeded with the same white light.
The measured signal is the difference between the probe intensity reflected by the excited sample and a reference signal originated by the same optical pulse. The time resolved signal has been acquired through a Lock-in amplifier.

Sample

The sample is a large and high-quality optimally doped Y-substituted Bi2212 single crystals ($Bi_2Sr_2Y_{0.08}Ca_{0.92}Cu_2O_{8+\delta}$), grown in an image furnace by the traveling-solvent floating-zone technique with a non-zero Yttrium content. The critical temperature is $T_c = 97$ K and the transition temperature is $T^* \sim 135$ K.

Laser Heating

The estimation of the sample heating due to the interaction with the pump pulse can be estimated using the linear absorption coefficient and assuming that all the absorbed energy results in a local increase of temperature. For the pump fluence related to the measurements presented in the main text ($f = 0.09$ mJ $\cdot$ cm^{-2}), the estimated sample heating is smaller than 2 K.
In order to avoid errors associated to erroneous estimate of the heating effects, we compared the transient reflectivity measurements at different photon energy and low temperature (80 K) and chose the pump fluences which gave the same time domain signal. We proceeded in the same way for the high fluence measurements describe in the following (see section 4).

PHASE DIAGRAM AND PUMP-PROBE MEASUREMENTS

We performed pump probe measurements on Yttrium doped Bi2212 (Y-Bi2212), $Bi_2Sr_2Y_{0.08}Ca_{0.92}Cu_2O_{8+\delta}$ at optimal doping, with superconducting phase for $T < T_c$ K, the pseudogap one for $T_c < T < T^*$ K and metallic one for $T > T^*$. As sketched in Figure 1, in time resolved measurement as a function of temperature all the phase contributions are visible and have a characteristic dynamics. In particular a "positive" dynamics is associated to the superconducting state, while a "deep" at about 1 ps is related to the pseudogap. This is the reason why we interpret an increase of the signal around 1 ps as an enhancement of the superconducting response.

In Figure 2 representative measurements at different pump photon energies and polarizations are reported. These data have been used in order to obtain the map difference in Figure 2 of the main text. The difference in the decay times between measurements at different photon energies is accounted for the duration of the pulse itself, which is different at different pump wavelengths. For low excitation energies the divergence of the decay time marks the critical temperature.

In order to compare the response at different energies around the critical temperature T_c, we considered the maximum value of the transient reflectivity at 97 K. The inset of Figure 3 shows the described analysis: it is clear that the red dots representing high photon energy nodal

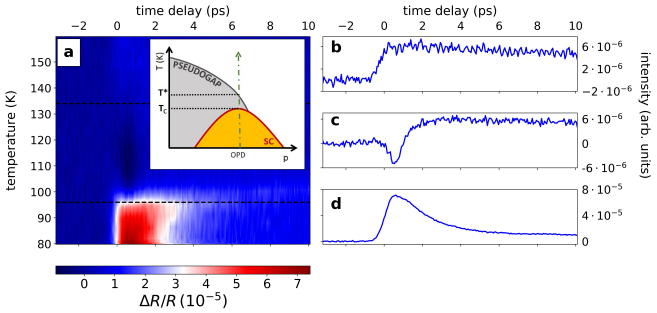

FIG. 1. a) Pump-probe measurement in temperature on Y-Bi2212, with high pump photon energy ($h\nu$ = 170 meV). Horizontal black lines represent the transition temperatures. In the inset a sketch of the phase diagram of the sample is shown; green dashed line highlight our doping value. b), c) and d) represent the transient reflectivity of the three phases (metallic, pseudogap and superconductive ones respectively).

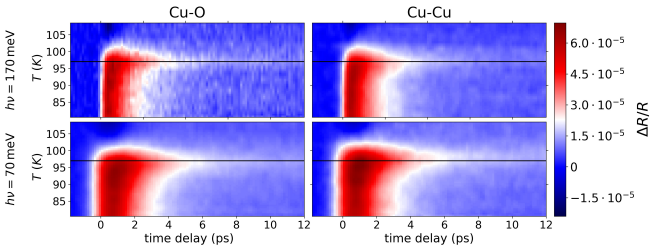

FIG. 2. Time resolved measurements in a smaller temperature range, in order to focus on the supercoductive-pseudogap phase transition. Measurements have been performed at different pump photon energies (170 and 70 meV, first and second row respectively), but same fluence, at two different pump polarizations.

and antinodal excitations are much closer to each other with respect to the low energy ones (blue spots).

Figure 3 shows the time dependence of the reflectivity subtraction between the different polarization cases shown in Figure 2. It is evident that, while the polarization does not affect the measurement with high pump photon energies excitations (flat red line centered at zero in Figure 3), the difference of low photon energies measurements present a non negligible time dependent signal. The result of the differential signal can be fitted with the same function used for the superconducting dynamics, that is a convolution between an exponential decay and a gaussian function, representing the cross correlation between pump and probe (black dashed line in Figure 3). From the fit procedure we could extract a value for the decay time, which is about 1.3 ps.

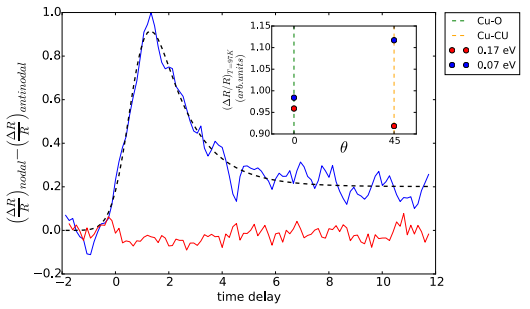

FIG. 3. Time dependence of the difference between nodal and antinodal excitation at a fixed temperature above T_c (we chose the temperature where the low photon energy signal reaches its maximum). The red and blue lines represent respectively high ($h\nu \approx 170$ meV) and low ($h\nu \approx 70$ meV) photon energy excitations, while the black dashed line is the fit of the latter. In the inset the maximum signal value at $T = 97$ K for both photon energies and polarizations is shown, in order to highlight the difference between the signals with different pump polarizations at low photon energies (θ is the angle between the Copper-Oxygen axis of the sample and the polarization of the pump).

HIGH FLUENCE MEASUREMENTS

The time resolved measurements shown in the main text (Figure 1 and 2) and in the previous section (Figure 2) have been performed with low pump fluence ($f = 0.09\,\mathrm{mJ\cdot cm^{-2}}$). In order to consolidate the physical picture emerging, i.e. that low photon energy excitations can trigger an increase of the superconducting signal above the equilibrium critical temperature, we have performed experiments at high excitation density ($f = 0.39\,\mathrm{mJ\cdot cm^{-2}}$). The results for high excitation density are plotted in Figure 4 for different photon energies, with pump and probe polarized along the Cu-Cu direction. In optical pump and probe experiments based on high probe photon energy (1.5 eV), photo-excitation with excitation density above critical value results in an additional pronounced response at longer times. This response was interpreted as non-thermal superconducting-to-normal state phase transition where the superconducting condensate is vaporized before the closing of the gap, leading to a transient inhomogeneous superconducting state.

Our measurements based on long wavelength photons reveal an overall similar response. On the other hand, from a comparison between the temperature dependence of the transient reflectivity (Figure 4) for photon energy comparable to 2Δ (Figure 4b) or much larger ($h\nu > 2\Delta$, Figure 4a) it appears evident that the positive $\frac{\Delta R}{R}$, which characterizes the superconducting phase, extends to significantly larger temperature for longer wavelengths. We stress that the two measurements were performed with similar absorbed fluence. These observations provide a

strong support to the scenario emerging from the paper.

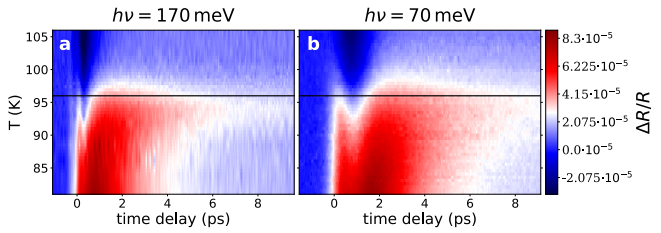

FIG. 4. Time resolved measurements with intense pump pulses (fluence $f = 0.39\,\mathrm{mJ}\cdot\mathrm{cm}^{-2}$) for two pump photon energies, polarized along the Cu-Cu direction. The black line represents the critical temperature $T_c = 97\,\mathrm{K}$

.

D-WAVE BCS MODEL: QUANTITIES AND METHODOLOGIES

The generalized BCS Hamiltonian mentioned in the main text has the following expression

$$\begin{aligned} H = &\sum_{\mathbf{k}} \varepsilon\left(\mathbf{k} - \frac{e}{\hbar}A(t)\boldsymbol{\epsilon}\right)\hat{n}(\mathbf{k}) \\ &+ \sum_{\mathbf{k}}\left(\Delta^*(\mathbf{k})\hat{\Psi}(\mathbf{k}) + \Delta(\mathbf{k})\hat{\Psi}^\dagger(\mathbf{k})\right), \end{aligned} \tag{1}$$

where $\varepsilon(\mathbf{k}) = -2t\left(\cos k_x + \cos k_y\right) - \mu$ is the two-dimensional tight-binding electronic dispersion with a nearest-neighbor hopping integral $t = 250$ meV and μ is the chemical potential, which has been fixed self-consistently in order to have a filling of $n = 0.9$.

The homogenous time-dependent vector potential of the pump pulse has the following expression

$$\begin{aligned} \mathbf{A}(t) &= A(t)\,\boldsymbol{\epsilon} \\ &= A_0 e^{\left(-\left(\frac{2\sqrt{\ln 2}(t-t_0)}{\tau}\right)^2\right)}\cos\left(\omega_0\left(t-t_0\right)\right)\boldsymbol{\epsilon} \end{aligned} \tag{2}$$

where A_0 is the intensity, which has been fixed to $1000\,\frac{\mathrm{meV\cdot fs}}{\mathrm{nm}}$ unless stated otherwise, $\tau = 200$ fs is the FWHM, ω_0 is the frequency, $\boldsymbol{\epsilon}$ is the in-plane polarization, which has been varied between nodal $\frac{1}{\sqrt{2}}(1,1)$ and antinodal $(1,0)$ configuration, and t_0 has been chosen such that $A(t=0) = 10^{-4}A_0$, so that one can use $A(t<0) = 0$ without incurring in any significant step-like change.

$\hat{n}(\mathbf{k}) = \sum_\sigma \hat{n}_\sigma(\mathbf{k})$, where $\hat{n}_\sigma(\mathbf{k}) = c^\dagger_\sigma(\mathbf{k})c_\sigma(\mathbf{k})$ is the number operator for spin σ of the Wannier electronic state with momentum $\mathbf{k}$, whose annihilation operator is $c_\sigma(\mathbf{k})$.

$\Delta(\mathbf{k}) = \zeta(\mathbf{k})\,|\Delta|\,e^{i\theta}$ is the gap function, where $\zeta(\mathbf{k}) = \frac{1}{2}\left(\cos k_x - \cos k_y\right)$ parametrizes the d-wave momentum dependence of the gap function, $|\Delta|$ is the amplitude of the gap parameter, θ is its phase. The amplitude of the gap parameter at $T = 0$ K has been set to $|\Delta(T = 0\,K)| = 25$ meV, while the phase of the gap parameter has been set to zero ($\theta = 0$ rad) at the equilibrium ($t < 0$ fs), for the sake of simplicity and without losing generality. The critical temperature is $T_c = 139.7$ K and the ratio between the zero-temperature gap parameter and the critical temperature gives $\frac{|\Delta(T=0\,K)|}{k_B T_c} = 2.08$, which is the typical d-wave BCS value. The temperature used is $T = 120$ K and the corresponding value of the gap at equilibrium is $|\Delta(T = 120\,K)| = 14.8315\,\mathrm{meV}$.

The pair operator mentioned in the main text is defined as $\hat{\Psi}(\mathbf{k}) = c_\uparrow(\mathbf{k})c_\downarrow(-\mathbf{k})$ and it is related to the gap function through the equation $\Delta(\mathbf{k}) = G\zeta(\mathbf{k})\sum_{\mathbf{k}'}\zeta(\mathbf{k}')\Lambda(\mathbf{k}')$, where G is the attractive BCS coupling constant and $\Lambda(\mathbf{k}) = \left\langle\hat{\Psi}(\mathbf{k})\right\rangle = |\Lambda(\mathbf{k})|\,e^{i\phi(\mathbf{k})}$ is the complex expectation value of the pair operator. The sum contained in the relation between $\Delta(\mathbf{k})$ and $\Lambda(\mathbf{k})$ explains why the induced phase incoherence of Λ shown in Figure 4f of the main text leads to an instantaneous suppression of the superconducting gap, despite the presence of pairing.

All calculations of the dynamical response have been performed within the density-matrix-theory framework, which gives the following set of relevant equations

$$\begin{cases} i\hbar\frac{\partial}{\partial t}\bar{n}(\mathbf{k}) = \Delta(\mathbf{k})\Lambda^*(\mathbf{k}) - \Delta^*(\mathbf{k})\Lambda(\mathbf{k}) \\ \\ i\hbar\dfrac{\partial}{\partial t}\Lambda(\mathbf{k}) = \left[\varepsilon\left(\mathbf{k} - \dfrac{e}{\hbar}\mathbf{A}(t)\right) + \varepsilon\left(\mathbf{k} + \dfrac{e}{\hbar}\mathbf{A}(t)\right)\right]\Lambda(\mathbf{k}) \\ \qquad\qquad + \Delta(\mathbf{k})\left[1 - 2\bar{n}(\mathbf{k})\right] \end{cases} \tag{3}$$

where $\bar{n}(\mathbf{k}) = \langle n_\uparrow(\mathbf{k})\rangle = \langle n_\downarrow(\mathbf{k})\rangle$.

It is worth noting that the coupling realized between the *Bloch/Wannier* electrons in a lattice and the electromagnetic field through the Peierls substitution, $\varepsilon\left(\mathbf{k} - \frac{e}{\hbar}A(t)\boldsymbol{\epsilon}\right)$, is

- intrinsically *non-linear* in the vector potential strength A and contains, a priori, all powers of A, reflecting the obvious difference with respect to the minimal coupling usually used for *free* electrons, containing terms up to A^2;
- intrinsically *anisotropic* as it reflects the anisotropy of the momentum space, borrowed by that of the direct space [$(0,1)/(1,0)$ bond direction vs $(1,1)$ diagonal direction], in a lattice.

In particular, we have that the first term in the expansion in powers of A appearing in the second equation above (i.e. at order A^2) couples the vector potential field, according to its actual polarization, to specific combinations of the components of the inverse mass tensor, which is anisotropic already for the very simple tight-binding dispersion used. Then, the indirect coupling through the

very same equation between the vector potential and the gap function $\Delta(\mathbf{k})$ also follows the anisotropic momentum dependence of this latter and puts such anisotropic momentum dependence in relation, through the properties of the actual dispersion $\varepsilon(\mathbf{k})$ and, in particular, of the inverse mass tensor, to the polarization of the vector potential. This rationalizes the possibility to explore through the polarization the dynamics of the gap function in different regions of the momentum space.

EFFECTIVE MODEL: PHOTON ENERGY DEPENDENCE

Figure 3b in the main text shows the photon energy dependence of the time-integrated value of the superconducting gap for nodal excitations; here we report the results of the calculations which originated them (Figure 5). The graphs represent the time dependence of the maximum values of the gap amplitude due to the pump excitation, both in nodal and antinodal configuration, for several pump photon energies. The difference between the time response of the superconducting signal in experiments and calculations related to the time decay (the increase of the superconducting signal lasts for some picoseconds in the measurements, while the enhancement of Δ follows the applied field in the calculations) is due to the absence of interactions in the microscopic model. Figure 5c shows the fluence dependence of the superconducting gap, for nodal (orange dots) and antinodal (green ones) excitations. Notice that while the nodal excitations leads to a linear increase of the gap with respect to the fluence, the decrease induced by an antinodal excitation is not linear at all and seems to saturate to a minimum value for high pump fluences.

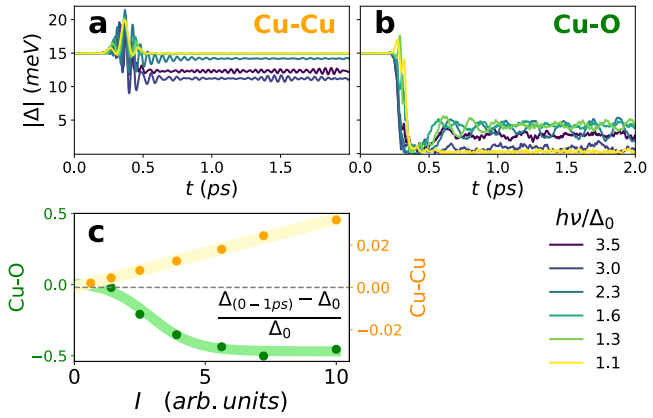

FIG. 5. a) and b) Time dependence of the maximum amplitude of the superconducting gap for different photon energies and polarizations of the pump. c) Integration of the gap amplitude in time (from 0 to 1 ps) as a function of the intensity of the applied fields (for photon energies $h\nu < 2\Delta$. Yellow and light green areas guide the eye.

* These two authors contributed equally
† Corresponding author: avella@physics.unisa.it
‡ Corresponding author: daniele.fausti@elettra.eu